Two-Level Distributed Voltage/Var Control of Aggregated PV Inverters in Distribution Networks

Article *in* IEEE Transactions on Power Delivery · November 2019

DOI: 10.1109/TPWRD.2019.2955506

5 authors, including:

Yu Wang
Nanyang Technological University
52 PUBLICATIONS **263** CITATIONS
SEE PROFILE

Tianyang Zhao
Nanyang Technological University
78 PUBLICATIONS **263** CITATIONS
SEE PROFILE

Chengquan Ju
Nanyang Technological University
10 PUBLICATIONS **71** CITATIONS
SEE PROFILE

Yan Xu
Nanyang Technological University
280 PUBLICATIONS **4,023** CITATIONS
SEE PROFILE

Two-Level Distributed Volt/Var Control using Aggregated PV Inverters in Distribution Networks

Yu Wang, *Member, IEEE,* Tianyang Zhao, *Member, IEEE,* Chengquan Ju, *Member, IEEE,* Yan Xu, *Senior Member, IEEE,* and Peng Wang, *Fellow, IEEE*

Abstract— **The penetration level of photovoltaic (PV) keeps increasing in modern distribution networks, which leads to various severe voltage limits violation problems. This paper aims to aggregate and utilize the PV inverters for voltage regulation by a fully distributed two-level Volt/VAr control (VVC) scheme. In the lower-level VVC (real-time scale), the rooftop PV inverters are aggregated via consensus algorithms and then governed by droop controllers in medium-voltage networks. The droop controller adjusts the reactive power output of each PV aggregator in real-time from its dispatched value depending on the bus voltage variations. In the upper-level VVC (15-min timescale), the reactive power of PV aggregators is dispatched for power loss minimization, where control signals are set as base values for PV aggregators. This problem is formulated as second-order cone programming and solved by the alternating direction method of multipliers. The simulation results demonstrate the effectiveness of the proposed method in both short-term and long-term scenarios with different system scales.[1]**

***Index Terms*— Distribution networks, Volt/VAr control, PV inverters, consensus algorithms, alternating direction method of multipliers.**

I. Introduction

A. Background and Motivation

In recent years, the penetration level of photovoltaic (PV) generation in power distribution networks keeps increasing rapidly [1]. In Australia, 21.6% of all houses now have a PV system installed, where Queensland and South Australia have more than 30% of houses having installed a PV system [2]. In Singapore, the PV penetration level is expected to increase to 25% by the year 2025 [3]. The *EcoCampus* project at Nanyang Technological University, Singapore demonstrates a practical example of the innovative campus with high PV penetration [4]. However, high penetration of PV generation will lead to various power quality issues, such as the widely recognized voltage rise and voltage fluctuation problems [5], [6]. The large-scale penetration of small capacity user-end PV systems is also challenging the control and operation framework of distribution networks, where more user-end devices become controllable via communication systems. In such circumstances, the control systems for electric grids are required to be more stable, resilient, flexible and secure [7]. Therefore, how to design an efficient voltage control scheme with the large-scale user-end PV penetration becomes an emerging and vital question to be investigated.

Given all the voltage regulation resources, the voltage regulation problem in distribution networks can be typically divided into two stages, which aims to control the slow and fast actuators separately [8], [9]. In the first stage, the voltage regulation is realized by mechanical devices such as on-load tap changers, step voltage regulators, and switched capacitors, etc. [9]. In order to reduce the frequency of taps/switches change and increase their lifetime, these mechanical devices are suggested to be manipulated in a longer time interval, e.g., hourly or even daily. In the second stage, the power inverters have much fast response speed and flexible operation ranges, therefore their reactive power is suitable for faster voltage regulation. The mechanical devices are to manage the basic network voltage profile based on PV/load predictions. Then the Volt/VAr control (VVC) of power inverters functions to adjust the voltage profiles considering real-time PV/load fluctuations. This paper focuses on the second-stage problem by a novel VVC scheme for aggregated PV inverters.

B. Related Works

According to the control architectures, VVC can be divided into three categories: i) decentralized, ii) centralized, and iii) distributed [10]. In decentralized (or called local) control, the power inverters can response to local voltage measurement at the point of common coupling (PCC) rapidly for local VVC. In [11], a PCC voltage droop control based VVC with its stability issue in distribution networks is presented. In [12], a multi-functional local VVC scheme is proposed for voltage quality issues caused by PV inverters. The local control schemes have the benefits of fast response speed, while it does not require communication infrastructures. However, the limitation of decentralized control is the lack of system-wide coordination, which can only provide non-optimal solutions. By contrast, centralized control aims to provide an optimal solution to VVC. In [9], a multi-time scale coordinated VVC scheme (hourly and 15 minutes) is proposed for high renewable-penetrated distribution networks. In [13], based on robust optimization, a three-stage VVC scheme, which includes mechanical devices scheduling, inverter output dispatch, and real-time droop control is proposed. However, the central controller suffers extensive computation and communication burdens, especially when dealing with a large

Y. Wang is with Rolls-Royce@NTU Corporate Lab, Nanyang Technological University, Singapore, 639798.

T. Zhao and C. Ju are with Energy Research Institute @ Nanyang Technological University, Singapore, 639798.

Y. Xu and P. Wang are with School of Electrical and Electronics Engineering, Nanyang Technological University, Singapore, 639798. (Corresponding author: Yan Xu, e-mail: xuyan@ntu.edu.sg)

number of control units; besides, it is inherently vulnerable to single-point communication failures; furthermore, the central controller needs to gather all the system information, which may not be always available in power distribution networks.

In recent years, the distributed control has shown its merits to overcome those limitations discussed above. The control and optimization objectives can be achieved in a distributed way with peer-to-peer communications, which have good plug-and-play capability and expendability [10]. In [8], a two-stage distributed control architecture of distributed inverters is proposed for network VVC. The authors in [14] propose a discrete-time consensus control of PV inverters to address voltage rise issues in low-voltage networks. In [15], a decentralized and distributed hybrid control scheme for PV inverters is proposed for both network voltage fluctuation and violation issues. The distributed consensus algorithms have also been used for the secondary voltage control of islanded microgrids [16], [17]. It should be noted that the voltage control problems in distribution networks and islanded microgrids have some different features: (i) In the hierarchical control framework of microgrids, the controllable DG units are operated as voltage sources with both P/f and Q/V droop control [18]. However, in distribution networks, the PV units with maximum power point tracking control are operated as current sources with reactive power related droop control [8], [14]. (ii) In islanded microgrids, the control objective is to restore all the bus voltages into a nominal value. In distribution networks with long feeders and heavy loads, the voltage control objectives turn to mitigate the voltage deviations and reduce power loss.

On top of the real-time control, reactive power should be optimally dispatched in the longer timescale. This problem can be formulated as the optimal power flow (OPF) problem and solved distributedly [19], [22], [23]. Typically, the branch flow model (i.e. *DistFlow*) is used to depict power flow in radial distribution networks [20]. The original OPF based on *DistFlow* can be turned into a convexified OPF by relaxing the nonlinear power loss term. Then the alternating direction method of multipliers (ADMM) can be applied to provide a distributed and fast-converged solution of the convex optimization problem [21]. Previous research has studied the convexified OPF problem and its distributed solution, such as [22], [23]. [19] provides a detailed review of formulation and solution methods for distributed OPF. In [22], by using the *DistFlow* and linearizing the nonlinear terms, a convex quadratic OPF is formulated to dispatch the reactive power from inverters. In [23], the original OPF is relaxed into second-order cone programming (SOCP) problem and exactness of the solution is discussed.

In practice, the capacity of single PV inverters is not enough to participate in the reactive power dispatch. Therefore, individual PV inverters should be assembled as aggregators to meet upstream network dispatch order. Existing distributed VVC methods either focus on the distributed optimization of distribution networks [22], [23] or the cooperative control of PV inverters [14], [15]. This paper aims at a distributed control framework considering both upper-level optimizations among aggregators and lower-level cooperative control within aggregators. From literature, this kind '*system of system*' problem is investigated by some recent research of networked microgrids [24], [25]. However, the fully distributed VCC scheme considering both inter and intra coordination for PV aggregators is of great importance but lack of investigation.

C. Contributions in This Paper

This paper proposes a two-level distributed and timescale coordinated VVC scheme for PV aggregators, aiming to bridge the gap between the upper-level optimal reactive power dispatch and lower-level real-time control. Compared to existing works in literature, major contributions are as follows:

(i) The proposed VVC scheme is fully distributed and includes two timescales coordinated control: i.e. upper-level and lower-level VVC. The PV uncertainty is handled by two timescale coordination (15 minutes dispatch and real-time adjustment), while the control system resilience is enhanced by the fully distributed control structure.

(ii) In the lower-level VVC, a distributed control approach is proposed to group each rooftop PV inverters at low-voltage (LV) side into aggregators. Then the aggregators are governed by the proposed droop controllers in medium-voltage (MV) networks. Note that most existing works only consider the inverters as one single inverter directly. In addition, the available reactive capacity of each aggregator is also estimated in a distributed manner.

(iii) In the upper-level VVC, based on the network conditions and available reactive power capacity, the aggregators are dispatched in a distributed way for network loss minimization. This problem is formulated as a SOCP and solved by ADMM. These optimal dispatch signals are updated every 15 minutes and set as base values for lower-level droop controls.

This paper is organized as follows. In Section II, the architecture of the proposed VVC is introduced. Next, the lower-level VVC and upper-level VVC are presented in detail in Section III and IV, respectively. The case studies with IEEE test systems are conducted and the simulation results are discussed in Section V. Finally, Section VI draws the conclusion.

II. Proposed VVC Architecture

A. System Overview

In this paper, a residential distribution network with high PV penetration is considered, as shown in Fig. 1. The rooftop PV inverters at the LV side are fed into a point of common coupling (PCC) and then connected to the MV network through an LV/MV transformer. In urban residual communities, it is reasonable to assume that the load demands are evenly distributed in each phase, and the building rooftop PVs are connected into the grid through three-phase AC/DC inverters [26]. Each group of PV inverters at the downstream of an MV/LV transformer is grouped into an aggregator via lower-level communication networks. The data exchange of

each bus in MV network is realized by an upper-level communication network. It motivates us to propose a VVC for the above scenario with only peer-to-peer communications. The state-of-the-art communication infrastructure in residential distribution networks including both cable communications and wireless technologies such as WiFi and Zigbee can enable this application [27]. Based on the above electrical and communication infrastructure, the research objective is to design a two-level fully distributed VVC scheme for aggregators of user-end PV inverters.

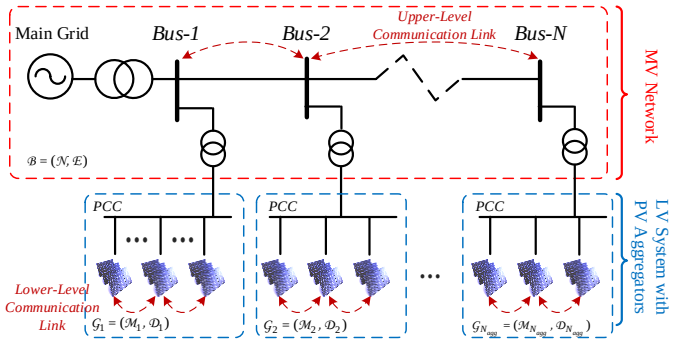

Fig. 1. Overview of the studied system.

Next, notations to describe the studied system are denoted. The radial MV distribution network is depicted by a tree graph $\mathcal{B} = (\mathcal{N}, \mathcal{E})$, which is assumed to be a three-phase balanced network. $\mathcal{N}=\{i \mid i=1, 2,\ldots, N\}$ represents the set of buses and $\mathcal{E}$ represents the set of distribution lines. The feed bus of the distribution network is numbered as 0. It is noted that there is a set of $\mathcal{N}_{agg}=\{k \mid k=1, 2,\ldots, N_{agg}\}$ ($\mathcal{N}_{agg} \subseteq \mathcal{N}$) PV aggregators in the MW network. The upper-level communication network has the same topology with the MV electrical network.

In aggregator k, the set of PV inverters are denoted as $\mathcal{M}_k$, which is denoted by $\mathcal{M}_k = \{j \mid j=1, 2,\ldots,M_k\}$. The aggregation of PV inverters is achieved by lower-level communication networks. The electrical network restraints are simplified as PV inverters are coupled by one PCC. The lower-level communication network of aggregator k is depicted by an undirected graph $\mathcal{G}_k = (\mathcal{M}_k, \mathcal{D}_k)$ with a set of nodes $\mathcal{M}_k$ and a set of edges $\mathcal{D}_k$. The nodes correspond to communication agents of PV inverters, and edges represent communication links for data exchange.

B. Architecture of Proposed VVC

The proposed two-level VVC has two coordinated timescales as shown in Fig.2: 15-mins and real-time. In 15-mins timescale, the objective is to minimize the network power loss within the operational voltage limits. The optimized dispatch signals are set as the base values for PV aggregators, which are updated every 15 minutes. The set of time steps is represented as $\mathcal{T}_d = \{0, \Delta t_d, 2\Delta t_d, \ldots, T_d\}$.

In the real-time scale, the network voltage fluctuations are more stochastic and should be mitigated by local droop control. For the droop control of each PV aggregator, a time-varying value based on each bus voltage will be added to the dispatched base value. Then, this combined control signal is further shared with each PV inverter within the aggregator in real-time. In addition, the reactive power constraint of each aggregator is also estimated for the upper-level VVC. The set of time steps is represented as $\mathcal{T}_s = \{0, \Delta t_s, 2\Delta t_s, \ldots, T_s\}$.

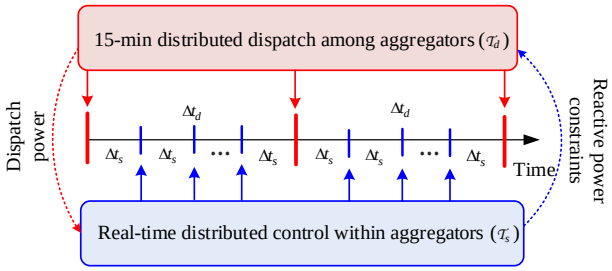

Fig. 2. Timescale coordination of the proposed two-level VVC.

III. Lower-Level VVC

In this section, the lower-level VCC is proposed for real-time operation and distributed reactive power sharing in each PV aggregator. The real-time control takes effect every 0.1s in this paper, and $t \in \mathcal{T}_s$.

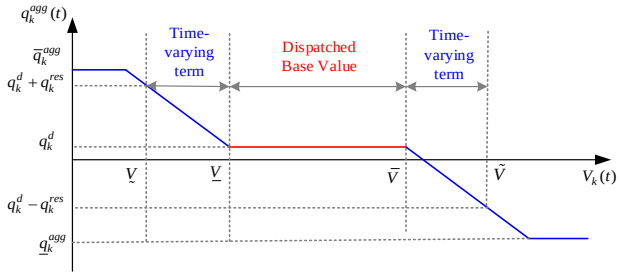

Fig. 3. The proposed droop control curve for PV aggregator.

A. Real-time VVC by Droop Control

The objective of the droop control is to mitigate the network voltage violations when the system operation point deviates far from the dispatched point. For example, during the period of cloud passing, the PV generation may be dramatically influenced, then the droop control can function to mitigate the voltage deviations. The working principle of droop control for real-time operation of PV aggregator is shown in Fig. 3. Depending on the bus voltage in the MV network, the reactive power output of the aggregator k is adjusted around the dispatch base value q_k^d in each dispatch period. If $V_k \in [\underline{V}, \bar{V}]$, the reactive power of the aggregator is kept at the dispatch base value q_k^d to minimize network loss. If $V_k \notin [\underline{V}, \bar{V}]$, a time-varying term has been activated to mitigate network voltage deviations. The total reactive power output q_k^{agg} of the aggregator k is represented as follows:

$$q_k^{agg}(t) = \begin{cases} q_k^d + G_k(V_k(t) - \bar{V}), & V_k(t) > \bar{V} \\ q_k^d, & \underline{V} \le V_k(t) \le \bar{V} \\ q_k^d + G_k(V_k(t) - \underline{V}), & V_k(t) < \underline{V} \end{cases} \quad (1)$$

where G_k is the droop control gain. $\underline{V}$ and $\bar{V}$ are the lower and upper bound to trigger the time-varying term of droop control.

Remark 1: The droop control gains are selected as $G_k = \alpha_k L_{kk}$, where $L_{kk} = \partial Q_k / \partial V_k$ is the sensitivity of bus voltage magnitude to the reactive power injection. To ensure the stability of the droop-controlled distribution networks, in general, $\alpha_k = 1/n_{bus}$ are selected as a reasonable gain value [8]. Besides, the voltage boundary $[\underline{V},\ \bar{V}]$ is typically selected as $[0.95, 1.05]$ according to [6], [9].

It should be also noted that the available capacity for droop control is the total reactive capacity of the aggregator subtracting the dispatched reactive power. Thus, a certain amount of capacity can be reserved during the dispatch period. By defining a critical voltage range as $[\underset{\sim}{V},\ \tilde{V}]$, the reactive power reserve of an aggregator q_k^{res} is calculated from:

$$q_k^{res} = \begin{cases} \bar{q}_k^{agg}, & q_k^{res} > \bar{q}_k^{agg} \\ G_k[\max(\underline{V} - \underset{\sim}{V}, \tilde{V} - \bar{V})], & \underline{q}_k^{agg} \le q_k^{res} \le \bar{q}_k^{agg} \\ \underline{q}_k^{agg}, & q_k^{res} < \underline{q}_k^{agg} \end{cases} \quad (2)$$

where $[\underset{\sim}{V},\ \tilde{V}]$ is selected as $[0.94, 1.06]$ in this paper; $\bar{q}_k^{agg}$ and $\underline{q}_k^{agg}$ are the upper and lower reactive power limits of the aggregator *k*.

B. Distributed Aggregation of PV Inverters

The droop controller of an aggregator is associated with a pinning node (called the leader). The leader updates a reference state $\mu_{k,0}$ for the aggregator *k* (depicted by graph $\mathcal{G}_k$) based on the reactive power output from droop control in (1) as follows:

$$\mu_{k,0}(t) = \frac{q_k^{agg}(t)}{M_k} \quad (3)$$

where $\mu_{k,0}$ is the reference state, M_k is the number of PV inverters in the aggregator *k*.

This reference state will be broadcasted to each PV inverter in the aggregator via communication graph $\mathcal{G}_k$ by the following leader-follower consensus control law:

$$\dot{\mu}_{k,j}(t) = \sum_{\hat{j}=1}^{M_k} a_{k,j\hat{j}}(\mu_{k,\hat{j}}(t) - \mu_{k,j}(t)) + g_{k,j}(\mu_{k,0}(t) - \mu_{k,j}(t)) \quad (4)$$

where $a_{k,j\hat{j}}$ represents the weight for information exchanged between inverter *j* and its adjacent inverter $\hat{j}$. $a_{k,j\hat{j}} = 1$ if inverters *j* and $\hat{j}$ are connected by an edge, otherwise, $a_{k,j\hat{j}} = 0$. $g_{k,j}$ represents the pinning gain, $g_{k,j} = 1$ if inverter *j* directly exchanges information from the leader, otherwise $g_{k,j} = 0$ [28].

The average values of upper and lower available VAr capacity for each inverter *j* ($\bar{\rho}_{k,j}$ and $\underline{\rho}_{k,j}$) of can be estimated from:

$$\begin{cases} \dot{\bar{\rho}}_{k,j}(t) = \bar{q}_{k,j}(t) + \sum_{\hat{j}=1}^{M_k} a_{k,j\hat{j}}(\bar{\rho}_{k,\hat{j}}(t) - \bar{\rho}_{k,j}(t)) \\ \dot{\underline{\rho}}_{k,j}(t) = \underline{q}_{k,j}(t) + \sum_{\hat{j}=1}^{M_k} a_{k,j\hat{j}}(\underline{\rho}_{k,\hat{j}}(t) - \underline{\rho}_{k,j}(t)) \end{cases} \quad (5)$$

where $\bar{q}_{k,j}$ and $\underline{q}_{k,j}$ are the upper and lower limits of available VAr capacity of inverter *j*, $\bar{\rho}_{k,j}$ and $\underline{\rho}_{k,j}$ are the estimated average values of upper and lower VAr limits.

Finally, based on (3)-(5), the reactive power output of each inverter *j* is calculated from:

$$q_{k,j}(t) = \begin{cases} \dfrac{\mu_{k,j}(t)}{\bar{\rho}_{k,j}(t)} \bar{q}_{k,j}(t), & \mu_{k,j}(t) > 0 \\ \dfrac{\mu_{k,j}(t)}{\underline{\rho}_{k,j}(t)} \underline{q}_{k,j}(t), & \mu_{k,j}(t) < 0 \end{cases} \quad (6)$$

where $q_{k,j}$ is the reactive power output of inverter *j* in aggregator *k*, which is within its operational limits as $q_{k,j}(t) \in [\underline{q}_{k,j}(t),\ \bar{q}_{k,j}(t)]$.

Remark 2: For a set of initial values and connected communication graph $\mathcal{G}_k$, the steady-state value of $q_{k,j}$ converges to

$$\lim_{t\to\infty} q_{k,j}(t) = \begin{cases} \dfrac{M_k \mu_{k,0}(0)}{\sum_{j=1}^{M_k} \bar{q}_{k,j}(0)} \bar{q}_{k,j}(0), & \mu_{k,j}(t) > 0 \\ \dfrac{M_k \mu_{k,0}(0)}{\sum_{j=1}^{M_k} \underline{q}_{k,j}(0)} \underline{q}_{k,j}(0), & \mu_{k,j}(t) < 0 \end{cases} \quad (7)$$

For practical implementation in discrete-time, there exists a $T_0 = k\Delta t_s$, for some accuracy level ε_1, such that

$$\begin{aligned} &\left\| \mu_{k,j}(t) - \mu_{k,0}(t) \right\| \le \varepsilon_1 \wedge \left\| \bar{\rho}_{k,j}(t) - \bar{\rho}_{k,\hat{j}}(t) \right\| \le \varepsilon_1 \\ &\wedge \left\| \underline{\rho}_{k,j}(t) - \underline{\rho}_{k,\hat{j}}(t) \right\| \le \varepsilon_1, \ \forall t \ge T_0, \ \ j, \hat{j} \in \mathcal{M}_k, t \in \mathcal{T}_s \end{aligned} \quad (8)$$

and the equilibrium in (7) is also achieved. The convergence analysis is given in Appendix-A.

C. VAr Capacity of PV Aggregator

The available VAr capacity of each PV inverter *j* in aggregator *k* is calculated from [9]:

$$q_{k,j}^{\max}(t) = \sqrt{(s_{k,j}^{PV})^2 - p_{k,j}(t)^2} \quad (9)$$

where $s_{k,j}^{PV}$ and $p_{k,j}$ are the rated capacity and real power output of a PV inverter, respectively.

Equivalently, (9) can be written as:

$$q_{k,j}^{\max}(t) = s_{k,j}^{PV} \sqrt{1 - \xi_{k,j}(t)} \quad (10)$$

where $\xi_{k,j}(t) = p_{k,j}(t) / s_{k,j}^{PV}$ is denoted as the PV generation factor. It is noted that the available VAr capacity is

represented as $[\underline{q}_{k,j}(t), \bar{q}_{k,j}(t)]$, which is only a subset of $[-q_{k,j}^{\max}(t), q_{k,j}^{\max}(t)]$ considering the user's local utilization.

The upper and lower limits of VAr capacity $\bar{q}_k^{agg}$ and $\underline{q}_k^{agg}$ in aggregator *k* are time-varying, which is equal to the sum of all PV inverters' available VAr capacity. However, these values cannot be directly calculated in a distributed way, as each node only knows its neighbors' information. As mentioned above, the leader can exchange information with inverter *j* if $g_{k,j} = 1$. Therefore, the upper and lower limits of VAr capacity of aggregator *k* can be acquired as follows:

$$\begin{cases} \bar{q}_k^{agg}(t) = \sum_{j=1}^{M_k} \bar{q}_{k,j}(t) \cong \dfrac{M_k \sum_{j=1}^{M_k} g_{k,j} \bar{\rho}_{k,j}(t)}{\sum_{j=1}^{M_k} g_{k,j}}, \\ \underline{q}_k^{agg}(t) = \sum_{j=1}^{M_k} \underline{q}_{k,j}(t) \cong \dfrac{M_k \sum_{j=1}^{M_k} g_{k,j} \underline{\rho}_{k,j}(t)}{\sum_{j=1}^{M_k} g_{k,j}}. \end{cases} \tag{11}$$

Thus, the operational limits of an aggregator $[\underline{q}_k^{agg}, \bar{q}_k^{agg}]$ are obtained from (11). This information is used to update the reactive power reserve in (2), and the distributed power dispatch in the next section.

IV. Upper-Level VVC

In the upper-level VVC, the reactive power output from PV aggregators is optimally dispatched in a longer timescale, i.e., 15mins, and $t \in \mathcal{T}_d$. The dispatch results will serve as the base value settings in droop control for each aggregator.

A. Power Flow in MV Distributed Networks

The feed bus of the MV distribution network is numbered as 1. Each bus $i \in \mathcal{N} \setminus \{1\}$ has a unique ancestor bus A_i, and a set of children buses C_i. All the neighbor bus of bus *i* is represented by $\hat{i} \in \mathcal{N}_i$. The line from bus A_i to bus *i* is labeled as line *i*, and $i \in \mathcal{E} = \{1, 2, ..., n\}$. For each bus $i \in \mathcal{N}$, $v_i = |V_i|^2$ represents the square of bus voltage. $s_i = p_i + jq_i$ is the complex power injection. For each line $i \in \mathcal{E}$, the line impedance is represented by $z_i = r_i + jx_i$. The complex power flow from bus A_i to bus *i* is $S_i = P_i + jQ_i$. The square of the line current is $l_i = |I_i|^2$.

For a radial MV distribution network $\mathcal{B}$, the power flow equations are represented as follows [22], [23]:

$$v_{Ai} = v_i + 2(r_i P_i + x_i Q_i) + l_i(r_i^2 + x_i^2), i \neq 1 \tag{12a}$$

$$P_i = \sum_{\hat{i} \in C_i} (P_{\hat{i}} + r_{\hat{i}} l_{\hat{i}}) + p_i^L + p_i^d \tag{12b}$$

$$Q_i = \sum_{\hat{i} \in C_i} (Q_{\hat{i}} + x_{\hat{i}} l_{\hat{i}}) + q_i^L + q_i^d \tag{12c}$$

$$P_i^2 + Q_i^2 = v_i l_i \tag{12d}$$

The reactive power constraint of each PV aggregator is:

$$\underline{q}_k^{agg} - q_k^{res} \le q_k^d \le \bar{q}_k^{agg} - q_k^{res} \tag{13}$$

The voltage magnitude should be within the constraints:

$$\underline{v}_i \le v_i \le \bar{v}_i \tag{14}$$

The quadratic equality constraint (13d) can be relaxed to a second-order cone form, and the relaxation is also exact as discussed by [23]:

$$P_i^2 + Q_i^2 \le v_i l_i \tag{15}$$

The upper-level VVC is to minimize the network loss subject to power flow equations and operational constraints. The objective function is defined as:

$$\sum_{i \in \mathcal{N}} f_i(x_i) = \sum_{i \in \mathcal{N}} r_i l_i \tag{16}$$

Therefore, the network loss minimization problem can be formulated as:

$$\min \sum_{i \in \mathcal{N}} r_i l_i \tag{17}$$

subject to: (12a)-(12c), (13)-(15)

B. Distributed Solution by ADMM

In this section, the ADMM algorithm is used to solve the relaxed optimization problem (17) in a distributed way [22], [29], [30]. The method iteratively minimizes the augmented Lagrangian over three types of variables: i) the primary variables; ii) the auxiliary variables to enforce boundary conditions among neighboring areas, and iii) the multipliers for dualizing the relaxed problem. The Lagrangian is designed to be separately relative to each type of variable so that we can cyclically minimize each variable while fixing the others. This allows us to solve the problem distibutedly and asymptotically converge to the same minimum costs obtained with centralized solvers.

For the specific problem in (17), the primary variable of node *i* is defined as $x_i = \{v_i, l_i, s_i, S_i\}$.

The auxiliary variable $y_{i\hat{i}}$ denotes variables of node $\hat{i}$ received by node *i*, which is defined as:

$$y_{i\hat{i}} = \begin{cases} (S_{ii}^{(y)}, l_{ii}^{(y)}, v_{ii}^{(y)}, s_{ii}^{(y)}) \ \hat{i} = i \\ (S_{iC_i}^{(y)}, l_{iC_i}^{(y)}), \hat{i} = C_i \\ (v_{iA_i}^{(y)}), \hat{i} = A_i \end{cases} \tag{18}$$

By substituting the original variables with the auxiliary variables, the explicit distributed form of (17) can be represented as follows:

$$\min \sum_{i \in \mathcal{N}} r_i l_i$$

$$\text{over: } \{x_i \mid i \in \mathcal{N}\}, \{y_{\hat{i}i} \mid i \in \mathcal{N}, \hat{i} \in \mathcal{N}_i\}$$

$$\text{s.t. } v_{A_i}^{(y)} = v_i^{(y)} + 2(r_i P_i^{(y)} + x_i Q_i^{(y)}) + l_i^{(y)}(r_i^2 + x_i^2), i \neq 1. \tag{19a}$$

$$P_i^{(y)} = \sum_{\hat{i}\in C_i}(P_{\hat{i}}^{(y)} + r_{\hat{i}} l_{\hat{i}}^{(y)}) + p_i^{L(y)} + p_i^{d(y)} \tag{19b}$$

$$Q_i^{(y)} = \sum_{\hat{i}\in C_i}(Q_{\hat{i}}^{(y)} + x_{\hat{i}} l_{\hat{i}}^{(y)}) + q_i^{L(y)} + q_i^{d(y)} \tag{19c}$$

$$\left|P_i^{(x)}\right|^2 + \left|Q_i^{(x)}\right|^2 \le v_i^{(x)} l_i^{(x)} \tag{19d}$$

$$\underline{q}_k^{agg} - q_k^{res} \le (q_k^d)^{(x)} \le \bar{q}_k^{agg} - q_k^{res} \tag{19e}$$

$$\underline{v}_i \le v_i^{(x)} \le \bar{v}_i \tag{19f}$$

$$x_i^{(x)} = y_{i\hat{i}}^{(y)} \tag{19g}$$

where the superscripts $(\cdot)^{(x)}$ and $(\cdot)^{(y)}$ on each variable denote whether the variable is updated in *X-update* or *Y-update*. The set of constraints in *X-update* is represented by $S_i^{(x)}$, and *Y-update* by $S_i^{(y)}$.

The augmented Lagrangian function of the above problem for each node is represented as:

$$L_{\rho,i}(x_i, y_{\hat{i}i}, \lambda_{i\hat{i}}) = f_i(x_i) + \sum_{\hat{i}\in\mathcal{N}_i}\left(\left\langle \lambda_{i\hat{i}}, x_i - y_{i\hat{i}}\right\rangle + \frac{\rho}{2}\left\|x_i - y_{i\hat{i}}\right\|_2^2\right) \tag{20}$$

where $\lambda_{i\hat{i}}$ is the Lagrangian multiplier for (20).

The optimization problem can be solved by the following steps based on ADMM:

[S1: *X-update*] Update primary variables by:

$$x_i^{m+1} = \arg\min_{x_i\in S_i^{(x)}} L_{\rho,i}(x_i, y_{i\hat{i}}^m, \lambda_{i\hat{i}}^m) \tag{21}$$

[S2: *Y-update*] Update auxiliary variables by:

$$y_{i\hat{i}}^{m+1} = \arg\min_{y\in S_i^{(y)}} L_{\rho,i}(x_i^{m+1}, y, \lambda_{i\hat{i}}^m) \tag{22}$$

[S3: λ *-update*] Update the multiplier by:

$$\lambda_{i\hat{i}}^{m+1} = \lambda_{i\hat{i}}^m + \rho(x_i^{m+1} - y_{i\hat{i}}^{m+1}) \tag{23}$$

Two metrics are defined as follows to check the convergence:

$$r^{m+1} = \left[\sum_{i\in\mathcal{N}}(x_i^{m+1} - y_i^{m+1})^2\right]^{1/2} \tag{24a}$$

$$s^{m+1} = \rho\left[\sum_{i\in\mathcal{N}}(y_i^{m+1} - y_i^m)^2\right]^{1/2} \tag{24b}$$

where r and s are primal and dual residuals. The iteration of [S1]-[S3] continues until r and s converge to the satisfied accuracy level ε_2.

Fig. 4 illustrates the information exchange between adjacent buses during this process. In *S1: X-update*, $y_{i\hat{i}}^m$ and $\lambda_{i\hat{i}}^m$ of the previous step from both children buses and ancestor buses are received by bus i. The argument of the minimum regarding primary variables is calculated from (21). In *S2: Y-update*, the updated primary variable x_i^{m+1} is exchanged to its adjacent buses. The argument of the minimum regarding auxiliary variables $y_{i\hat{i}}^{m+1}$ is calculated from (22). Finally, in *S3:* λ *-update*, $\lambda_{i\hat{i}}^m$ is updated by (23) with only local information.

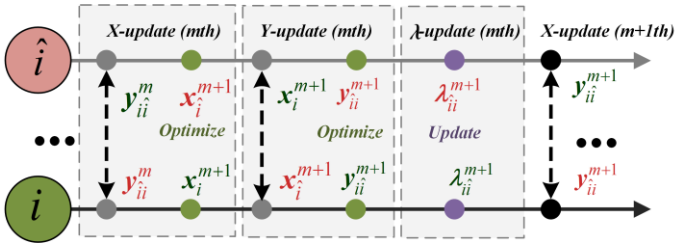

Fig. 4. Data exchange among adjacent nodes in the ADMM.

Remark 3: The convergence of the upper-level distributed optimization depends on the selection of ρ and network scale. As pointed in [29] and [30], the network diameter has a stronger impact than the network size on the rate of convergence. With the low-bandwidth communication infrastructures, this algorithm can be converged between two dispatch intervals. Besides, the proposed method is initially designed for balanced MV networks. For the unbalanced MV network, the proposed method could be modified based on the methods in [22], [30]. The droop control and PV aggregation also need to be performed as per phase voltage conditions.

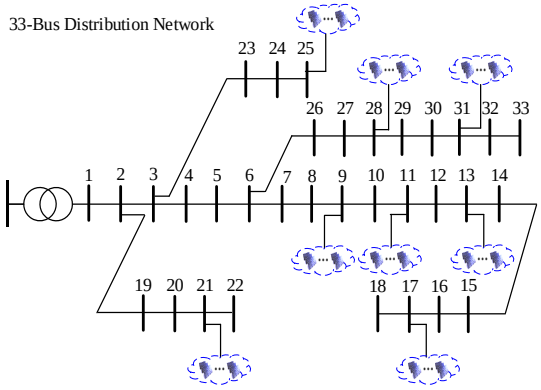

Fig. 5. Diagram of the IEEE 33-bus radial distribution network.

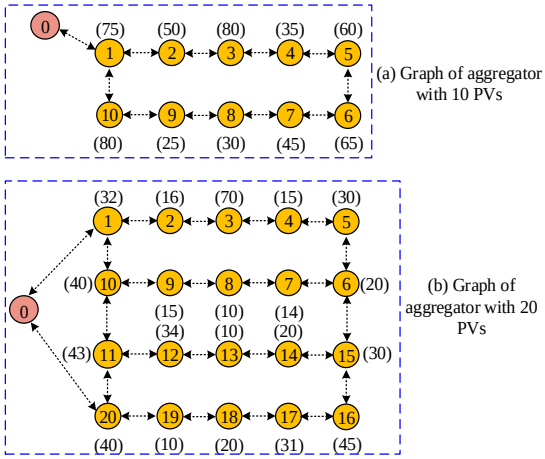

Fig. 6. The communication graphs of the PV aggregators: (a) aggregator with 10 PVs, (b) aggregator with 20 PVs.

V. Simulation Results

A. Test System and Parameter Settings

In this paper, two IEEE test distribution networks i.e. 33-bus system and 69-bus system are used to test the proposed VVC method [31]. The single line diagram of the IEEE 33-bus system is shown in Fig. 5. There are 8 PV aggregators located at different buses. It should be noted that the placement and size of PV units and the inverters have an impact on results, which is determined at the planning stage [32]. In this paper, two types of PV aggregators with the capacity of 550kVA are considered: (a) aggregator with 10 PVs and (b) aggregator with 20 PVs. The communication graphs and the capacity of each PV inverter (in kW) are shown in Fig. 6. In this test, the substation voltage is 1.0 p.u., the operational voltage range is $[\underline{V},\ \bar{V}]=[0.95, 1.05]$ and the critical voltage range is $[\underline{V},\ \tilde{V}]=[0.94, 1.06]$. Besides, the single line diagram of the IEEE 69-bus system is shown in Fig. 7, where there are 15 PV aggregators with the capacity of 550kVA spread in the system. The simulation is conducted in Matlab with Gurobi solver.

In the following subsections, the convergence for each control level of the proposed VVC is discussed first. Then both long timescale (24-hour) and short timescale (one-hour) simulations are carried out to validate the proposed VVC. Two case studies are conducted with different test systems (i) Case A: IEEE 33-bus system. (ii) Case B: IEEE 69-bus system.

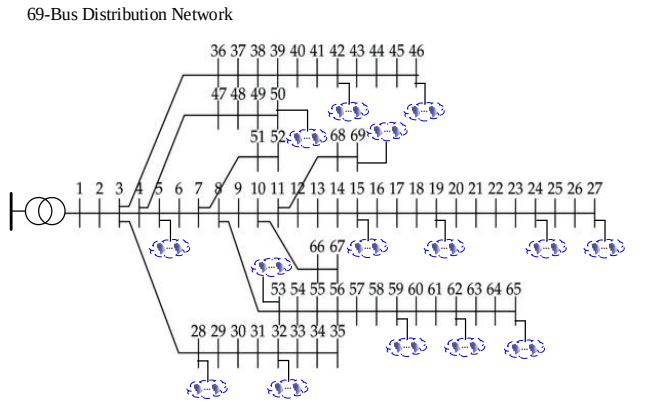

Fig. 7. Diagram of the IEEE 69-bus radial distribution network.

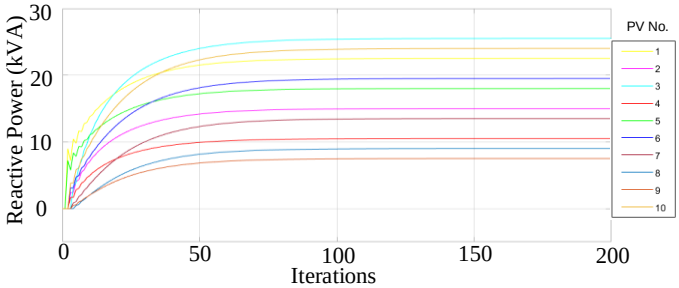

Fig. 8. Convergence of distributed aggregation control for the aggregator with 10 PVs.

B. Convergence

As an important concern of distributed algorithms, the algorithm convergence is investigated in this section. Generally, the convergence of the distributed consensus algorithms is highly related to the weights and topology of communication networks as well as the location of the leader. The convergence of distributed aggregation control for PV aggregators with the communication graph in Fig. 6 (a) is demonstrated in Fig. 8. The PV generation factor is considered as 0.8, therefore, the reactive capacity of each aggregator is $550\times\sqrt{1-0.8^2}=330$ kVA according to (10). The total reactive power increases from 0 to 165 kVA at the start of the simulation. The results demonstrate that the distributed control of PV aggregators can reach the steady-state within 100 iterations, and the power-sharing is proportional to their capacity given in Fig. 6 (a). As the lower-level VVC is a dynamic algorithm, the reference signals from droop control can be continuously updated without waiting for convergence.

In the upper-level dispatch, the convergence of ADMM is related to the network scale and parameter of ρ. The primal and dual residuals (r and s) of the upper-level optimization for the 33-bus system are shown in Fig. 9. The results show that with a properly chosen of ρ, the algorithm can reach a high accuracy in hundreds of iterations. For the same signal exchange rate of 0.1s as above, the algorithm can surely find the optimal solution within the 15-min dispatch interval of upper-level control. In Table I, the iteration number respect to different parameters ρ and two networks for primal and dual residuals to reach the accuracy of ε_2<2e-3 are given. Generally, a smaller ρ will lead to fast convergence, but the solution accuracy will be influenced if ρ is too small.

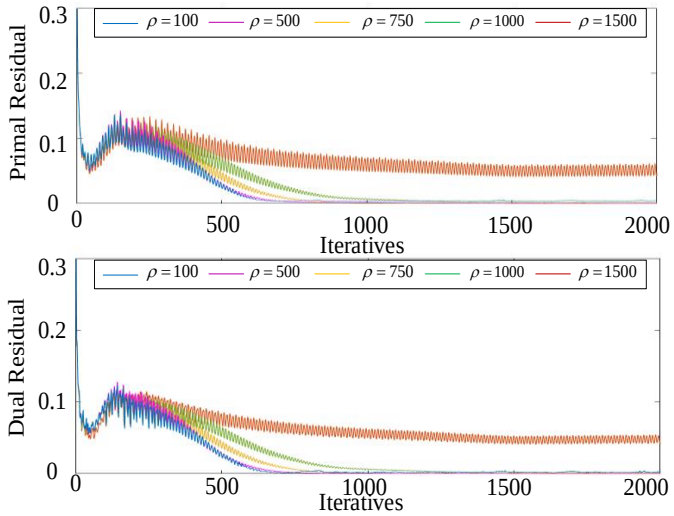

Fig. 9. Primal and dual residuals of distributed optimization based on ADMM.

Table I Iteration Number for Convergence of ADMM

Value of ρ	200	500	750	1000	1500
Iterations for ε_2<2e-3 (33-bus network)	691	705	890	1238	>2000
Iterations for ε_2<2e-3 (69-bus network)	786	795	962	1350	>2000

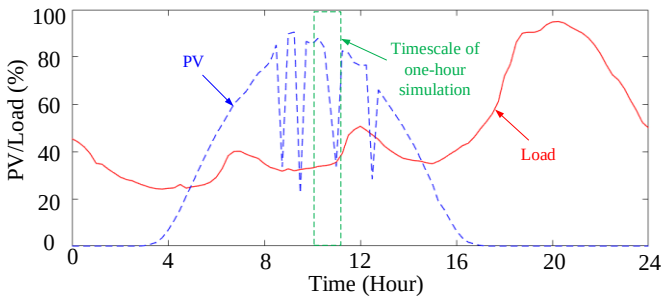

Fig. 10. 24-hour PV and load profiles with 15-minute sampling rate.

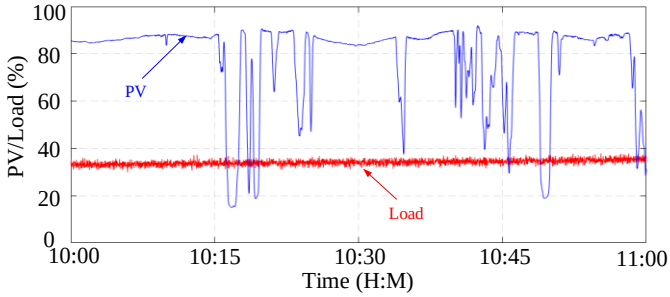

Fig. 11. One-hour PV and load profiles with 1-second sampling rate.

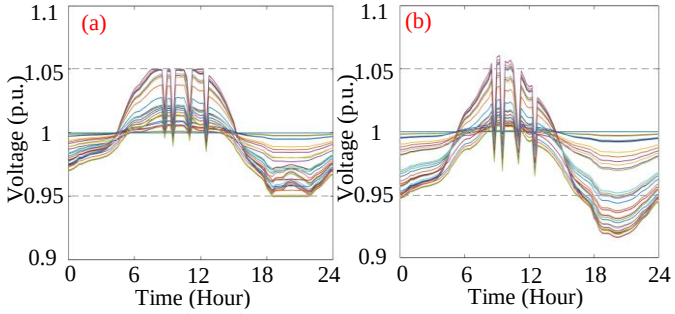

Fig. 12. Voltage profiles of the 33-bus distribution network in Case A-1. (a) with the proposed VVC; (b) without the proposed method.

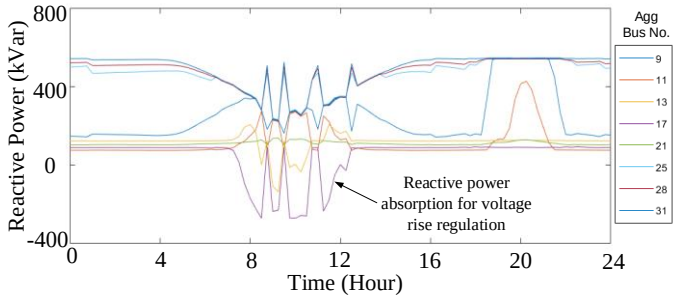

Fig. 13. Reactive power dispatched to each aggregator in Case A-1.

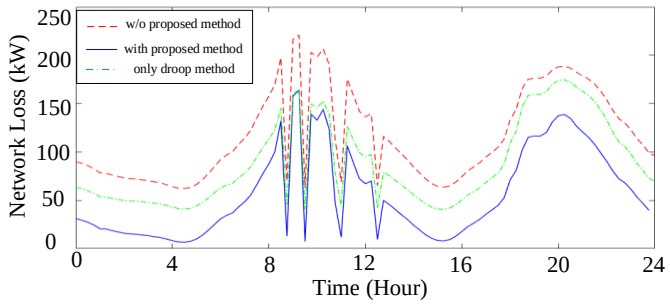

Fig. 14. Network power loss (i) with the proposed VVC (ii) without the proposed VVC and (iii) with only droop control in Case A-1.

C. Case A: 33-bus Networks

The 24-hour PV and load data with 15-min sampling rate are shown in Fig. 10 [33], [34]. The high-resolution PV and load data from 10:00 to 11:00 with 1-second sampling rate is shown in Fig. 11. These two timescales of PV and load data are used for short-term and long-term simulations.

1) Case A-1: Long-Term Simulation

The results of 24-hour simulation in *Case A-1* are shown in Figs. 12-14. The voltage profiles of the 33-bus distribution network with and without the proposed control scheme are compared in Fig. 12. All the bus voltages are regulated within $[0.95, 1.05]$ by the upper-level dispatch. Correspondingly, each aggregator will provide the dispatched reactive power output, as shown in Fig. 13. During high PV generation periods, a portion of aggregators in the distribution network needs to absorb some reactive power for voltage rise regulation. The network power loss, as the optimization objective of the upper-level, is minimized during the operation period. Fig. 14 compares the network power loss (i) with the proposed VVC (ii) without the proposed VVC and (iii) with only Q-V droop control. The 24-hour total network energy loss (time integration of power loss) is 1.68 MWh, which is far less than that without the proposed VVC of 3.36MWh. The total network energy loss with only droop control is 2.65MWh.

2) Case A-2: Short-Term Simulation

The results of one-hour simulation in *Case A-2* are demonstrated in Figs. 15-18. As shown in Fig. 15, the proposed VVC can effectively control the network voltages, even though there are fluctuations between two dispatch points. The droop control defined in (1) will take effect when the bus voltage is out of the normal operational range $[\underline{V}, \bar{V}] = [0.95, 1.05]$. For each dispatch time instant (every 15 minutes), the optimal reactive power output of each aggregator will be dispatched by the upper control level. If the voltage cannot be maintained within $[0.95, 1.05]$, the droop control is functioned to mitigate the PV fluctuations during one dispatch period. It can be observed that in Fig. 16 the base value of each aggregator is changed every 15 minutes. The reactive power is further shared by each PV inverter within one aggregator. As an example, the reactive power-sharing by each PV inverter of the PV aggregator at bus 17 (Aggregator-17) is shown in Fig. 17. Each inverter in Aggregator-17 shares the reactive power requirements from the proposed VVC according to their capacity rating given in Fig. 6 (a).

In addition, to illustrate that the proposed control structure is resilient with plug-and-play of PVs caused by either manual operations or communication failures, a comparison study has been made and shown as Fig. 18. In this condition, PV-10 is plugged out from 10:13 to 10:19, while PV-7 is plugged out from 10:32 to 10:38. It can be found that during the periods of one PV plugged out, the rest of the PVs will increase their outputs to meet the total reactive requirement. It indicates the outside characteristics of the PV aggregators can remain the same even though there are PV plugged in and out operations.

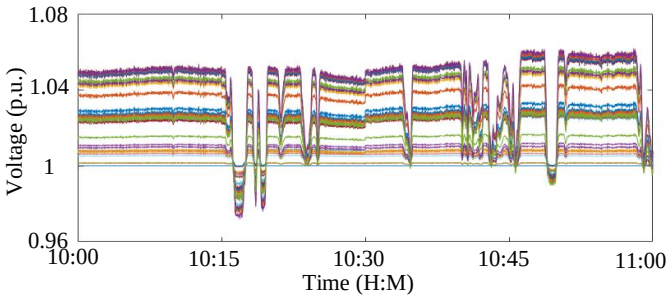

Fig. 15. Voltage profiles of the 33-bus distribution network in Case A-2.

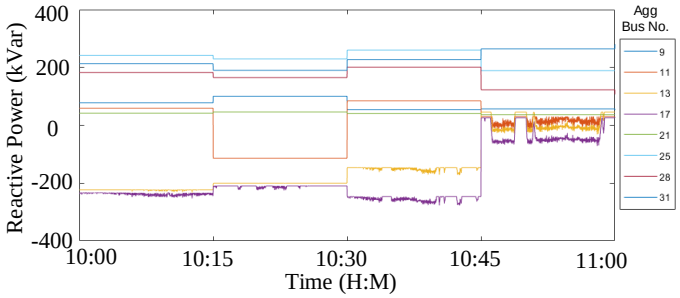

Fig. 16. Reactive power injection of each aggregator in MV distribution networks in Case A-2.

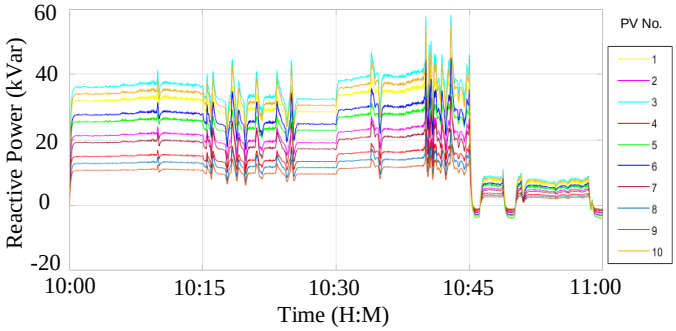

Fig. 17. PV reactive power absorption in Aggregator-17 with 10 PVs in Case A-2.

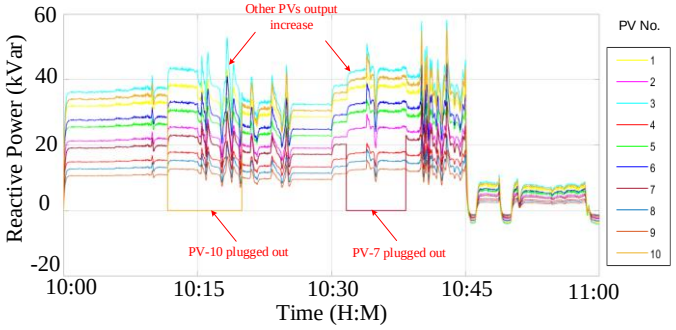

Fig. 18. Plug-and-play operation of PVs in Case A-2.

D. Case B: 69-bus Networks

In *Case B*, the proposed method is validated in a larger network IEEE 69-bus system with 15 PV aggregators, as shown in Fig. 7. The 24-hour and one hour PV and load data in *Case A* given by Figs. 9 and 10 are still utilized in this test case.

1) Case B-1: Long-Term Simulation

The results of 24-hour simulation in *Case B-1* are shown in Figs. 19-21. The voltage profiles of the 69-bus distribution network with and without the proposed control scheme are compared in Fig. 19. All the bus voltages are regulated within $[0.95, 1.05]$ by the upper-level dispatch. Each aggregator can provide the dispatched reactive power output, as shown in Fig. 20. Fig. 21 compares the network power loss (i) with the proposed VVC (ii) without the proposed VVC and (iii) with only Q-V droop control. The 24-hour total network energy loss (areas of power loss) is 2.16 MWh, which is far less than that without the proposed VVC of 3.1MWh. The total network energy loss of with droop control is 2.8MWh.

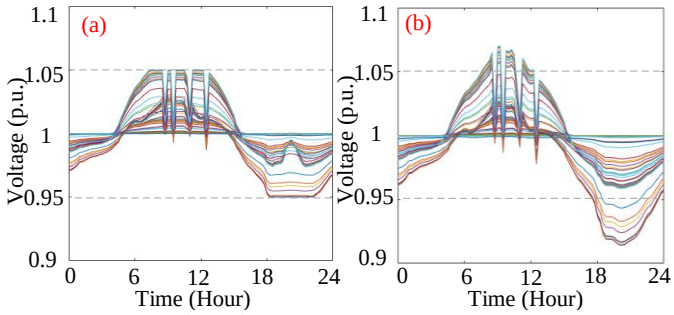

Fig. 19. Voltage profiles of the 69-bus distribution network in Case B-1. (a) with the proposed VVC; (b) without the proposed method.

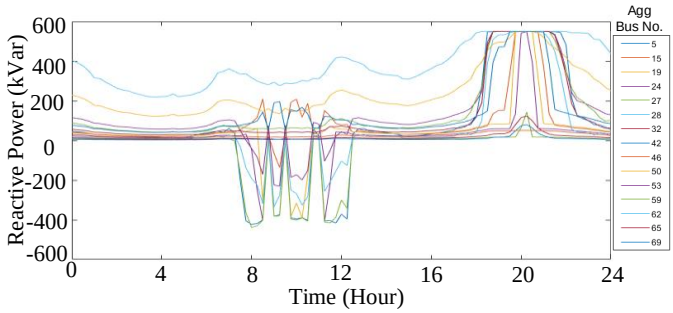

Fig. 20. Reactive power dispatched to each aggregator in Case B-1.

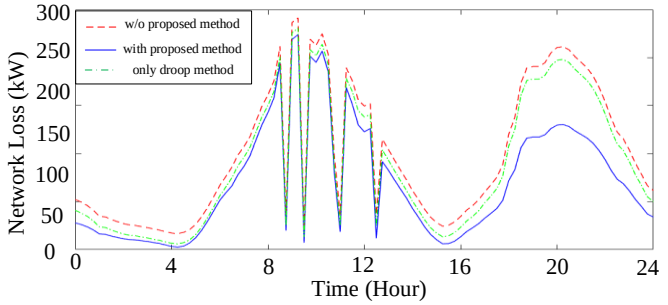

Fig. 21. Network power loss (i) with the proposed VVC (ii) without the proposed VVC and (iii) with only droop control in Case B-1.

2) Case B-2: Short-Term Simulation

The results of one-hour simulation in *Case B-2* are shown in Figs. 22-24. Similar to *Case A*, as shown in Fig. 22, the proposed VVC can effectively control the network voltage variations. In Fig. 23, the base value of each aggregator is changed for every 15 minutes, and the droop control takes effect for the aggregators when there are bus voltage violations.

In addition, the larger PV aggregator with 20 PVs is further considered in this case. The capacity and communication graph of the studied PV aggregator are shown in Fig. 6 (b). As shown in Fig. 24, each PV can provide reactive power proportional to their capacity to meet the total reactive power requirement of Aggregator-27 in Fig. 23.

In summary, the proposed VVC can handle both short-term and long-term voltage regulation in a fully distributed manner. All the reactive power reserves from PV inverters are effectively utilized to handle the voltage problems bring along with high PV penetration. The total network loss as an objective of the proposed VCC is minimized. The proposed method demonstrates a reliable and efficient way to manage and control of PV inverters in future high PV penetrated distribution networks.

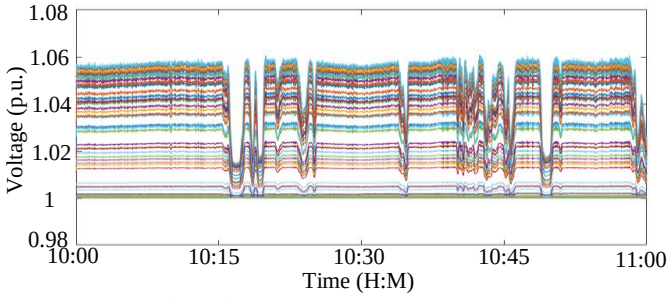

Fig. 22. Voltage profiles of the 69-bus distribution network in Case B-2.

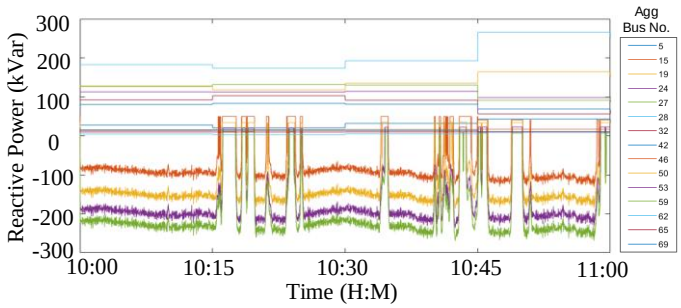

Fig. 23. Reactive power injection of each aggregator in MV distribution networks in Case B-2.

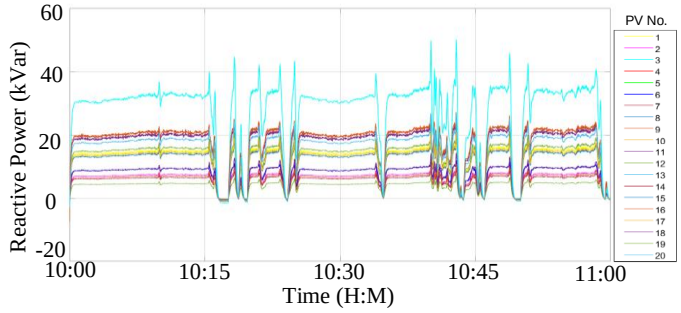

Fig. 24. PV reactive power absorption in Aggregator-27 with 20 PVs in Case B-2.

VI. Conclusion

In this paper, a two-level distributed VVC scheme for high PV penetrated distribution networks is proposed. Compared with centralized approaches, the proposed VVC enhances the system resilience as its distributed architecture. Various case studies have been conducted to validate the effectiveness of the proposed control scheme. The results demonstrate that the network voltage regulation is achieved in two timescales by the proposed two-level VVC. The network loss is reduced with the upper-level dispatch of aggregators within the voltage constraints, while the PV fluctuations between the dispatch intervals are handled by the droop control in the lower-level in real-time. The reactive power of one aggregator is further shared by each PV inverter according to their capacity. Besides, the convergence, flexibility and scalability issues are also discussed. The proposed method provides a feasible solution for fully distributed control and management of PV inverters in power distribution networks.

Appendix

A. Converge Analysis

The distributed control law in (4) is based on leader-follower consensus algorithms [28]. If the communication graph $\mathcal{G}_k$ is connected, (4) can converge to a unique solution:

$$\lim_{t\to\infty}\mu_{k,j}(t)=\mu_{k,0}(0) \tag{25}$$

The distributed control law in (5) is based on dynamic average consensus algorithms [35]. If the communication graph $\mathcal{G}_k$ is connected, (5) can converge to the unique solutions:

$$\lim_{t\to\infty}\bar{\rho}_{k,j}(t)=\frac{1}{M_k}\sum_{j=1}^{M_k}\bar{q}_{k,j}(0) \tag{26}$$

$$\lim_{t\to\infty}\underline{\rho}_{k,j}(t)=\frac{1}{M_k}\sum_{j=1}^{M_k}\underline{q}_{k,j}(0) \tag{27}$$

According to the proposed control in (6), if $\mu_{k,j}(t)>0$, it can be derived that

$$\lim_{t\to\infty}q_{k,j}(t)=\frac{\lim_{t\to\infty}\mu_{k,j}(t)}{\lim_{t\to\infty}\bar{\rho}_{k,j}(t)}\bar{q}_{k,j}(0)=\frac{\mu_{k,0}(0)}{\frac{1}{M_k}\sum_{j=1}^{M_k}\bar{q}_{k,j}(0)}\bar{q}_{k,j}(0) \tag{28}$$

Similarly, if $\mu_{k,j}(t)<0$, it can be derived that

$$\lim_{t\to\infty}q_{k,j}(t)=\frac{\lim_{t\to\infty}\mu_{k,j}(t)}{\lim_{t\to\infty}\underline{\rho}_{k,j}(t)}\underline{q}_{k,j}(0)=\frac{\mu_{k,0}(0)}{\frac{1}{M_k}\sum_{j=1}^{M_k}\underline{q}_{k,j}(0)}\underline{q}_{k,j}(0) \tag{29}$$

Therefore, combining (28) and (29), we can obtain the steady-state equilibrium in (7).

References

[1] Renewables 2018 Golbal Status Report. [Online]. Available: http://www.ren21.net/status-of-renewables/global-status-report/.

[2] Solar Trends Report for Solar Citizens. [Online]. Available: http://apvi.org.au/wp-content/uploads/2018/12/Solar-Trends-Report-for-Solar-Citizens-FINAL_11-12-18_2_logos.pdf.

[3] Eco-Business website. [Online]. https://www.eco-business.com/news/singapore-could-be-25-solar-powered-by-2025/.

[4] Ecocampus project. [Online]. Available: http://ecocampus.ntu.edu.sg/Pages/index.aspx.

[5] A. Samadi, et al. "Coordinated active power-dependent voltage regulation in distribution grids with PV systems," *IEEE Transactions on Power Delivery*, vol. 29, no .3, pp. 1454-1464, Jan. 2014.

[6] Y. Wang, et al. "Coordinated control of distributed energy-storage systems for voltage regulation in distribution networks," *IEEE Transactions on Power Delivery*, vol. 31, no .3, pp. 1132-1141, Jul. 2015.

[7] N. Mahmud, and A. Zahedi, "Review of control strategies for voltage regulation of the smart distribution network with high penetration of

renewable distributed generation," *Renewable Sustainable Energy Reviews*, vol. 64, pp: 582-595, Oct. 2016.
[8] B. A. Robbins, et al. "A two-stage distributed architecture for voltage control in power distribution systems," *IEEE Transactions on Power Systems*, vol. 28, no. 2, pp.1470-1482, May 2013.
[9] Y. Xu, Z. Y. Dong, R. Zhang, and D. J. Hill, "Multi-timescale coordinated voltage/var control of high renewable-penetrated distribution networks," *IEEE Transactions on Power Systems*, vol. 32, no. 6, pp. 4398-4408, Feb. 2017.
[10] K. E. Antoniadou-Plytaria, et al. "Distributed and decentralized voltage control of smart distribution networks: models, methods, and future research," *IEEE Transactions on Smart Grid*, vol. 8, no .6, pp. 2999-3008, Nov. 2017.
[11] P. Jahangiri and D. C. Aliprantis, "Distributed volt/var control by PV inverters," *IEEE Transactions on Power Systems*, vol. 28, no. 3, pp. 3429-3439, Aug. 2013.
[12] M. J. E. Alam, K. M. Muttaqi, and D. Sutanto, "A multi-mode control strategy for VAr support by solar PV inverters in distribution networks," *IEEE Transactions on Power Systems*, vol. 30, no. 3, pp. 1316-1326, May 2015.
[13] C. Zhang, Y. Xu, Z. Dong, and J. Ravishankar "Three-Stage Robust Inverter-Based Voltage/Var Control for Distribution Networks with High-Level PV," *IEEE Transactions on Smart Grid*, vol. 10, no. 1, pp. 782-793, Sep. 2017.
[14] G. Mokhtari, et al. "Smart robust resources control in LV network to deal with voltage rise issue," *IEEE Transactions on Sustainable Energy*, vol. 4, no .4, pp. 1043-1050, Oct. 2013.
[15] Y. Wang, et al. "Decentralized-distributed hybrid voltage regulation of power distribution networks based on power inverters," *IET Generation, Transmission and Distribution*, vol. 13, no. 3, pp. 444-451, Nov. 2018.
[16] A. Bidram, A. Davoudi, F. L. Lewis, and J. M. Guerrero, "Distributed cooperative secondary control of MGs using feedback linearization," *IEEE Transactions on Power Systems*, vol. 28, no. 3, pp. 3462-3470, Aug. 2013.
[17] F. Guo, et al. "Distributed secondary voltage and frequency restoration control of droop-controlled inverter-based MGs," *IEEE Transactions on Industrial Electronics*, vol. 62, no .7, pp. 4355-4364, Jul. 2015.
[18] Y. Wang, et. al. "Cyber-Physical Design and Implementation of Distributed Event-Triggered Secondary Control in Islanded Microgrids," *IEEE Transactions on Industry Applications*, vol. 55, no. 6, pp. 5631-5642, Nov.-Dec. 2019.
[19] D. K. Molzahn, et al. "A survey of distributed optimization and control algorithms for electric power systems," *IEEE Transactions on Smart Grid*, vol. 8, no .6, pp. 2941-2962, Nov. 2017.
[20] M. Baran and F. Wu, "Optimal capacitor placement on radial distribution systems," *IEEE Transactions on Power Delivery*, vol. 4, no. 1, pp. 725–734, Jan. 1989.
[21] S. Boyd, N. Parikh, E. Chu, B. Peleato, and J.Eckstein, "Distributed optimization and statistical learning via the alternating direction method of multipliers," *Foundations and Trends® in Machine learning*, vol. 3, no. 1, pp. 1–122, 2011.
[22] B. A. Robbins, and A. D. Domínguez-García, "Optimal reactive power dispatch for voltage regulation in unbalanced distribution systems," *IEEE Transactions on Power Systems*, vol. 31, no .4, pp. 2903-2913, Jul. 2016.
[23] M. Farivar and S. H. Low, "Branch flow model: Relaxations and convexification—Part I," *IEEE Transactions on Power Systems*, vol. 28, no. 3, pp. 2554–2564, Aug. 2013.
[24] W. Zhang, and Y. Xu, "Distributed Optimal Control for Multiple Microgrids in a Distribution Network," *IEEE Transactions on Smart Grid*, in press, 2018.
[25] Y. Liu, et al. "Distributed Optimal Tie-Line Power Flow Control for Multiple Interconnected AC Microgrids," *IEEE Transactions on Power Systems*, in press, 2018.
[26] Solar inverter solutions for building applications, ABB. [Online]. Available:https://library.e.abb.com/public/26cbca93f85d4ffc9652cc4cd93c83c3/ABB_BCB00139%20Rev.C_Brochure_Solar%20Inverter%20solutions%20for%20building%20applications_EN_2019.pdf.
[27] V. C. Gungor, et al. "Smart grid technologies: Communication technologies and standards," *IEEE Transactions on Industrial Informatics*, vol. 7, no .4, pp. 529-539, Nov. 2011.
[28] H. Zhang, F. L. Lewis, and Z. Qu, "Lyapunov, adaptive, and optimal design techniques for cooperative systems on directed communication graphs," *IEEE Transactions on Industrial Electronics*, vol. 59, no. 7, pp. 3026–3041, 2012.
[29] Q. Peng and S. H. Low, "Distributed optimal power flow algorithm for radial networks, I: Balanced single phase case," *IEEE Transactions on Smart Grid*, vol. 9, no. 1, pp.111-121, Apr. 2016.
[30] Q. Peng and S. H. Low, "Distributed algorithm for optimal power flow on an unbalanced radial network," *54th IEEE Conference on Decision and Control (CDC)*, 2015.
[31] M. E. Baran and F. F. Wu, "Network reconfiguration in distribution systems for loss reduction and load balancing," *IEEE Transactions on Power Delivery*, vol.4, no. 2, pp. 1401–1407, Apr. 1989.
[32] Y. Zhang, Y. Xu, H.M. Yang, and Z.Y. Dong, "Voltage Regulation-Oriented Co-Planning of Distributed Generators and Battery Storage in Distribution Networks," *Int. J. Electrical Power and Energy Systems*, vol. 105, pp. 79-88, Feb. 2019.
[33] 1-second resolution data, EPRI. [Online]. Available: http://dpv.epri.com/measurement_data.html.
[34] J. A. Jardini, et al. "Daily load profiles for residential, commercial and industrial low voltage consumers," *IEEE Transactions on Power Delivery*, vol. 15, no .1, pp. 375-380, 2000.
[35] R. Olfati-Saber, J. A. Fax, and R. M. Murray, "Consensus and Cooperation in Networked Multi-Agent Systems," *Proceedings of the IEEE*, vol. 95, no. 1, pp. 215-233, Mar. 2007.

Yu Wang (S'12-M'17) received the B.Eng. degree from Wuhan University, Wuhan China in 2011, and the M.Sc. and Ph.D. degree from Nanyang Technological University, Singapore in 2012 and 2017, respectively. He is currently a research fellow in Nanyang Technological University, Singapore. His research interests include distributed control and optimization, energy storage systems, microgrids and smart grids.

Tianyang Zhao (S'14–M'18) received the B.Eng., M.Eng. and Ph.D. degrees in electrical engineering from North China Electric Power University, Beijing China in 2011, 2013 and 2017, respectively. Currently, he is a Postdoctoral Research Fellow with Energy Research Institute, Nanyang Technological University, Singapore. His research interests include power system operation optimization, game theory and reliability.

Chengquan Ju received the B.Eng. degree in electrical engineering from Wuhan University, Wuhan, China, in 2012 and the M.Sc degree in power engineering from Nanyang Technological University (NTU), Singapore, in 2013. He is currently an optimization engineer in Envision Digital. His research interests include energy management, optimal power flow, energy storage planning, hybrid energy system and hierarchical and distributed optimization.

Yan Xu (S'10-M'13) received the B.E. and M.E degrees from South China University of Technology, Guangzhou, China in 2008 and 2011, respectively, and the Ph.D. degree from The University of Newcastle, Australia, in 2013. He is now the Nanyang Assistant Professor at School of Electrical and Electronic Engineering, Nanyang Technological University (NTU), and a Cluster Director at Energy Research Institute @ NTU (ERI@N), Singapore. Previously, he held The University of Sydney Postdoctoral Fellowship in Australia. His research interests include power system stability and control, microgrid, and data-analytics for smart grid applications. Dr Xu is an Editor for IEEE TRANSACTIONS ON SMART GRID, *CSEE Journal of Power and Energy Systems*, and an Associate Editor for *IET Generation, Transmission & Distribution*.

Peng Wang (M'00-SM'11-F'17) received his B.Sc. degree from Xi'an Jiaotong University, China, in 1978, the M. Sc. degree from Taiyuan University of Technology, China, in 1987, and the M. Sc. and Ph.D. degrees from the University of Saskatchewan, Canada, in 1995 and 1998 respectively. Currently, he is a professor of Nanyang Technological University, Singapore.